6494 *Biochemistry* **2010,** *49,* 6494–6503
DOI: 10.1021/bi100299r

BIOCHEMISTRY
including biophysical chemistry & molecular biology
Article

Structurally Designed *trans*-2-Phenylcyclopropylamine Derivatives Potently Inhibit Histone Demethylase LSD1/KDM1[†,‡,§]

Shinya Mimasu,[∥,⊥] Naoki Umezawa,[@] Shin Sato,[∥] Tsunehiko Higuchi,[@] Takashi Umehara,*[,∥] and Shigeyuki Yokoyama*[,∥,⊥]

[∥]*RIKEN Systems and Structural Biology Center, 1-7-22 Suehiro-cho, Tsurumi, Yokohama 230-0045, Japan,* [⊥]*Department of Biophysics and Biochemistry, Graduate School of Science, The University of Tokyo, 7-3-1 Hongo, Bunkyo-ku, Tokyo 113-0033, Japan, and* [@]*Graduate School of Pharmaceutical Sciences, Nagoya City University, 3-1 Tanabe-dori, Mizuho-ku, Nagoya, Aichi 467-8603, Japan*

Received March 1, 2010; Revised Manuscript Received June 11, 2010

ABSTRACT: Lysine-specific demethylase 1 (LSD1/KDM1) demethylates histone H3, in addition to tumor suppressor p53 and DNA methyltransferase 1 (Dnmt1), thus regulating eukaryotic gene expression by altering chromatin structure. Specific inhibitors of LSD1 are desired as anticancer agents, because LSD1 aberrations are associated with several cancers, and LSD1 inhibition restores the expression of abnormally silenced genes in cancerous cells. In this study, we designed and synthesized several candidate compounds to inhibit LSD1, based on the structures of LSD1 and monoamine oxidase B (MAO-B), in complex with an antidepressant tranylcypromine (2-PCPA) derivative. Compound S2101 exhibited stronger LSD1 inhibition than tranylcypromine and the known small LSD1 inhibitors in LSD1 demethylation assays, with a k_{inact}/K_I value of 4560 M^{-1} s^{-1}. In comparison with tranylcypromine, the compound displayed weaker inhibition to the monoamine oxidases. The inhibition modes of the two 2-PCPA derivatives, 2-PFPA and S1201, were identified by determination of the inhibitor-bound LSD1 structures, which revealed the enhanced stability of the inhibitor−FAD adducts by their interactions with the surrounding LSD1 residues. These molecules are potential pharmaceutical candidates for cancer or latent virus infection, as well as research tools for LSD1-related biological investigations.

Post-translational modifications of histone tails, including methylation, acetylation, and phosphorylation, are important pieces of epigenetic information that control eukaryotic chromatin structure and gene expression (*1*, *2*). Methylation of histone tails is unique among all of the epigenetic modifications because it can facilitate both transcriptional activation and repression, depending on the specific lysine or arginine residues modified. In contrast, other modifications typically only activate or repress transcription. Several lysine and arginine methylation sites have been mapped on histone H3, and many of them are regulated by methyltransferases and demethylases. Histone H3 lysine 9 (H3K9) and histone H3 lysine 27 are transcriptionally repressive modifications inducing heterochromatin formation (*3*−*5*), which is a state of highly condensed nucleosomes. On the other hand, histone H3 lysine 4 (H3K4) is a transcriptionally active modification (*6*). H3K4 can be mono-, di-, or trimethylated, depending on the methylase. For example, MLL1 acts as a methyltransferase for H3K4me3, whereas Jarid1C, a member of the JmjC domain-containing enzymes, demethylates di- and trimethylated H3K4 (*6*, *7*). Among the demethylases, lysine-specific demethylase 1 (LSD1/KDM1) was the first identified histone demethylase, which removes one or two methyl groups from H3K4 in an FAD-dependent manner (*8*−*11*). LSD1 requires the corepressor CoREST to demethylate mono- or dimethylated H3K4 in the nucleus (*12*, *13*) and also interacts directly with HDAC1 and -2 proteins to form functional complexes in this state within the nucleus (*13*, *14*). The LSD1−CoREST complex is repressed by BHC80, which recognizes nonmethylated H3K4 using the PHD domain and prevents the LSD1−CoREST complex from accessing the histone H3 tail (*15*). LSD1 not only demethylates H3K4me2 but also demethylates H3K9me2 when complexed with the androgen receptor, the prostate cancer-related p53-K370, which regulates p53-53BP-dependent apoptosis, and DNA methyltransferase 1 (Dnmt1), controlling DNA methylation (*16*−*18*). LSD1 is involved in the regulation of many cancerous cells, such as breast, colon, prostate, and neural cancer cells (*16*−*21*), and in viral gene activation (*22*) and thus is regarded as a promising drug target protein.

Several LSD1 inhibitors have been reported. Biguanide and bisguanidine polyamine analogues, which inhibit polyamine oxidase in the FAD-dependent enzyme family, reportedly block LSD1 and allow re-expression of aberrantly silenced genes in colon carcinoma cells (*20*, *21*). The combined use of the polyamine analogues with DNA methyltransferase inhibitors represents a promising anticancer treatment for colon tumors (*20*, *21*). The monoamine oxidase (MAO) inhibitors,

[†]This work was supported by the Program for Promotion of Fundamental Studies in Health Sciences of the National Institute of Biomedical Innovation (NIBIO) of Japan to T.U. and in part by the Targeted Proteins Research Program (TPRP) from the Ministry of Education, Culture, Sports, Science and Technology (MEXT) of Japan to S.Y. S.M. is a research fellow of the Japan Society for the Promotion of Science (JSPS).

[‡]Structural coordinates have been deposited in the Protein Data Bank, as entries 3ABT (LSD1−2-PFPA) and 3ABU (LSD1−S1201).

[§]The patent application covering the compounds described in this study was filed with as patent JP 2008-91436 on March 31, 2008.

*To whom correspondence should be addressed. E-mail: umehara@gsc.riken.jp or yokoyama@biochem.s.u-tokyo.ac.jp. Phone: +81-45-503-9457. Fax: +81-45-503-9201.

 Published on Web 06/22/2010

including the antidepressant tranylcypromine (also known as *trans*-2-phenylcyclopropylamine hydrochloride, 2-PCPA, or Parnate), also inhibit LSD1 (*23*−*27*), impair neuroblastoma cell growth (*28*), and block viral gene expression (*22*). 2-PCPA reacts with the FAD inside the MAO reaction cavity, and the MAO-B−2-PCPA complex structure revealed that the cyclopropyl moiety of 2-PCPA splits and fuses to C(4)a of FAD (*29*). Because LSD1 also possesses FAD in its reaction cavity, 2-PCPA was considered to inhibit LSD1 in a similar fashion, by forming a covalent bond with LSD1-FAD. The LSD1 structures inhibited by 2-PCPA revealed that 2-PCPA was fused to FAD via a covalent five-membered ring, as reported by Yang et al., and/or partially formed a covalent bond to the N(5) site of FAD, as we reported, in the LSD1 catalytic center (*26*, *27*). However, despite its potency, 2-PCPA shows greater inhibition of MAOs, such as MAO-A and MAO-B (*23*, *24*). Therefore, the compounds must be improved, in terms of their specificity for LSD1 and their potential side effects with other FAD-dependent enzymes. In this study, we designed a series of 2-PCPA derivatives based on the 2-PCPA-inhibited structures of LSD1 (*26*, *27*) and MAO-B (*29*) and identified several compounds that specifically block LSD1 more potently than the known LSD1 inhibitors. Finally, we determined the crystal structures of LSD1 inhibited by two of the potent inhibitors, to gain further insight into drug design.

MATERIALS AND METHODS

Chemical Compounds. The synthesis of *trans*-2-pentafluorophenylcyclopropylamine hydrochloride (2-PFPA) is described in the Supporting Information. The *trans*-2-phenylcyclopropylamine hydrochloride (2-PCPA) was purchased from BIOMOL International (Philadelphia, PA). Other 2-PCPA derivatives were purchased from ChemGenesis, Inc. (Tokyo, Japan). The general methods for the synthesis of these 2-PCPA derivatives, and the synthesis of the hit inhibitory compounds, S1201, S1402, S2101, S2107, and S2111, are described in the Supporting Information.

Proteins and Peptides. The hexahistidine-tagged LSD1 protein for biochemical assays was prepared as follows. The pET Duet-LSD1 plasmid, expressing the region encoding amino acids 172−833, was transformed into Rosetta (DE3) *Escherichia coli* (Novagen). The cells were grown to late log phase at 37 °C and then were induced overnight with 0.3 mM IPTG at 20 °C. The cells were lysed by sonication in 20 mM Tris-HCl buffer (pH 8.5), containing 0.5 M NaCl, 20 mM imidazole, and 1 mM DTT. The supernatant fraction was loaded onto a HisTrap HP column (GE Healthcare), and the fraction containing the LSD1 protein was eluted with a linear imidazole gradient, using 20 mM Tris-HCl (pH 8.5), 0.5 M NaCl, 0.5 M imidazole, and 1 mM DTT as the elution buffer. The eluted LSD1 fractions were further purified by gel filtration on a HiLoad 16/60 Superdex 200 column (GE Healthcare), with 20 mM HEPES-NaOH buffer (pH 7.5), containing 0.3 M NaCl and 2 mM DTT. The LSD1 protein was eluted as a single peak, and the fractions were pooled and concentrated to approximately 4 mg/mL. The LSD1 protein used for crystallization was prepared in essentially the same manner described previously (*26*). The recombinant human MAO-A and MAO-B proteins were purchased from Sigma-Aldrich (M7316 and M7441, respectively). The K4-dimethylated H3 peptide (H3K4me2, corresponding to amino acids 1−20) for the LSD1 demethylase inhibition assay was purchased from Toray Research Center, Inc. (Kamakura, Japan).

LSD1 Inhibition Assays. The kinetic inhibition parameters of LSD1 demethylase inhibition were obtained using the peroxidase-coupled reaction method. The LSD1 protein (3.0 pmol) was incubated with 40 μM H3K4me2 peptides, in a buffer containing 10 mM HEPES-Na (pH 7.5), 200 μM 4-aminoantipyrine, the Modified Trinder's reagent TOOS [*N*-ethyl-*N*-(2-hydroxy-3-sulfopropyl)-3-methylaniline, sodium salt, dihydrate], and 0.01 mg/mL horseradish peroxidase, for 10 min. This system generates a k_{cat} of 7.61 ± 0.56 min^{-1} and a K_m of 16 ± 5 μM. The horseradish peroxidase converts TOOS and 4-aminoantipyrine, using the peroxidase byproduct produced by LSD1 demethylation, to a pink/violet-colored compound, with a λ_{max} of 555 nm (http://www.dojindo.co.jp/protocol/protocol/trinder.pdf). The reaction mixture was prepared in the dark to inhibit the reactivity of the Trinder's reagent. The absorption of the reaction mixture was measured at 562 nm every 10 s with a microplate reader (Ultrospec Visible Plate Reader II 96, GE Healthcare). Although the λ_{max} for TOOS is 555 nm, measuring the wavelength at 562 nm was sufficient to provide accurate results of the inhibition, since the equations used to calculate K_I are dependent on the difference in activity, and not the absolute values. The results were transformed to the amounts of demethylated peptides for LSD1, and oxidized tyramine for MAOs, using the ε value for TOOS of 3.92×10^4. The results were analyzed and fit with the slow-binding inhibitor equation (eq 1) to yield k_{obs} and were further transformed to calculate k_{inact} and K_{Iapp} according to the Kitz−Wilson analysis, or with an offset value k_{offset} when the *y*-intercept was clearly non-zero (eq 2) (*26*−*31*). K_{Iapp} was transformed to K_I to exclude the bias from substrate concentrations (eq 3) (*26*). Data were fit with GraFit (http://www.erithacus.com/grafit/) and KyPlot (http://www.kyenslab.com/jp/). Each result was calculated from at least three individual experiments.

$$\text{product} = v_0(1 - e^{-kt})/k + \text{offset} \quad (1)$$

$$k_{obs} = (k_{inact})/[1 + K_{I(inact)app}/[I]] + k_{offset} \quad (2)$$

$$K_{I(inact)app} = K_{I(inact)}(1 + S/K_m) \quad (3)$$

MAO Inhibition Assays. MAO inhibition assays were performed using the peroxidase-coupled reaction method, in essentially the same manner described for LSD1, but with 40 or 50 μM tyramine as the substrate and 9.0 and 4.5 μg of MAO-A and MAO-B, respectively. The results were analyzed and calculated in the same manner described for LSD1. Each result was calculated from at least three individual experiments. The symbols plotted on the time course assays are the averages of the experiments, and the best-fit line was calculated and fit by the slow-binding inhibitor equation, using KyPlot.

Structural Analysis. Crystals of the LSD1 complexes with the inhibitors 2-PFPA and S1201 were formed by cocrystallization. Each inhibitor (250 μM) was individually cocrystallized with 3 mg/mL LSD1 in 100 mM HEPES-Na buffer (pH 7.5), containing 5% 2-methyl-2,4-pentanediol and 3.5−4.0% (w/v) polyethylene glycol monomethyl ether 2000, at 4 °C. The crystals were harvested after 3 weeks. X-ray diffraction data were collected on the BL26B2 and BL41XU beamlines at SPring-8. The LSD1 inhibitor crystals of 2-PFPA and S1201 diffracted to 3.2 and 3.1 Å, respectively. The diffraction data were processed and scaled using the HKL2000 package and XDS. The LSD1 structures were determined by molecular replacement with Phaser, using the native form of LSD1 [Protein Data Bank (PDB) entry 2Z5U] as the starting model. The electron density was clear and well-phased, because the molecular replacement

model was determined at 2.25 Å. The model was manually modified and refined by using Cuemol (http://cuemol.sourceforge.jp/en/), Pymol (http://pymol.sourceforge.net/), Coot (*32*), and CNS (*33*, *34*). Both structures fit suitably with the Ramachandran plot, using Rampage in the CCP4 program suite (*35*). The structures had 93.4 and 90.1% of the residues in the favored region, 5.9 and 8.5% in the allowed region, and 0.6 and 1.4% in the outlier area for 2-PFPA and S1201, respectively. The chemical structures and names of the conjugate between 2-PFPA and flavin adenine dinucleotide (FAD) and the conjugate between S1201 and FAD are provided as Supporting Information (Figure S1).

Western Blot Analysis of Compound-Treated Cells. HEK293T cells (RIKEN BRC RCB2202; kindly provided by M. Wakiyama) were grown in 100 mm dishes in Dulbecco's modified Eagle's medium (Gibco BRL, catalog no. 11995), containing 10% FBS (ICN Biomedicals Inc., catalog no. 2916754, lot. no. 7457F) and a 100 units/mL penicillin, 100 μg/mL streptomycin antibiotic solution (Nacalai Tesque, catalog no. 26253-84) under a 5% CO_2 atmosphere at 37 °C. Cells at approximately 70% confluency were treated with LSD1 inhibitors for 24 h, detached, and rinsed several times with ice-cold PBS. Nuclear extracts were prepared using a CelLytic NuCLEAR extraction kit (Sigma-Aldrich), according to the manufacturer's instructions. Each nuclear extract was electrophoresed on a 10 to 20% SDS−polyacrylamide gel and then transferred to a nitrocellulose membrane (Hybond-ECL, Amersham Biosciences). The proteins on the membranes were probed with primary antibodies (anti-H3, Abcam ab1791; anti-H3K4me2, Upstate 07-030; and anti-LSD1, Abcam ab17721) and then with a secondary antibody (goat anti-rabbit IgG−horseradish peroxidase conjugates, Santa Cruz Biotechnology, sc-2004) and were detected with a chemiluminescent system, Immobilon Western (Millipore, P90720). The band intensities were visualized with an image analyzer, LAS-1000plus (Fujifilm).

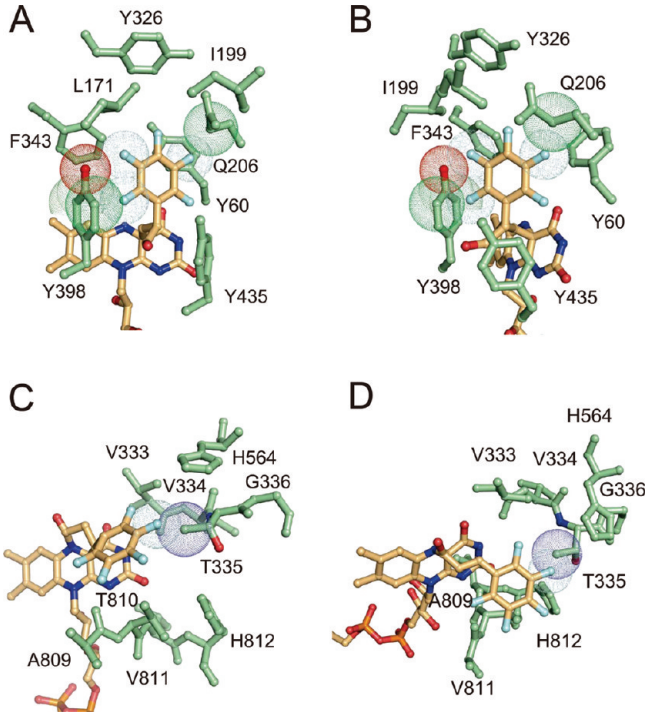

FIGURE 1: Structural superimpositions of MAO-B and LSD1 with a 2-PCPA derivative, later designated as 2-PFPA. (A and B) Structural comparisons of the MAO-B−2-PCPA complex with fluorine atoms. (B) Structure rotated horizontally by 30° from panel A. (C and D) Structural comparisons of the LSD1−2-PCPA complex with hypothetical fluorine atoms in the phenyl ring of 2-PCPA. (D) Structure rotated vertically by 30° from panel C. Dotted spheres represent hypothetical steric clashes. Green and orange sticks indicate LSD1 residues and LSD1-FAD, respectively. Cyan atoms represent hypothetical fluorines. MAO-B forms a different adduct with 2-PCPA in comparison to LSD1, in that the MAO-B adduct forms a covalent bond at FAD C(4)a whereas LSD1 forms covalent bonds at both N(5) and C(4)a. Note that the MAO-B adduct clashes with Y398 and F343 from one side, and Q206 from the other side, whereas the LSD1 adduct clashes with T335 from only one side.

RESULTS

Design and Inhibition Analysis of 2-PFPA. To design selective LSD1 inhibitors, we first designed the 2-PCPA derivatives with a halogen, such as fluorine, in the phenyl ring, because fluorine substituents are nonreactive and can also induce hydrogen bonds with neighboring carbonyl atoms (*36*). Furthermore, fluorine is often used to replace H in organic molecules, but the sizes and stereoelectronic influences of the two atoms are quite different (*36*). Therefore, the introduction of a fluorine substituent would enable compound modification with fewer anomalous interactions. We thus superimposed the 2-PCPA derivatives with fluorines in the phenyl ring on the crystal structures of 2-PCPA-inhibited LSD1 (PDB entry 2Z5U) and MAO-B (PDB entry 1OJB), to identify the discrepancies in their inhibitory states (Figure 1). Because LSD1 fuses at C(4)a and N(5) of FAD to form a five-membered ring (*26*, *27*) and MAO-B forms a different complex, fused only at the C(4)a site (*29*), we could potentially make 2-PCPA derivatives that react selectively with LSD1. We hypothesized that an inhibitor would exhibit enhanced specificity for LSD1 if the phenyl ring of 2-PCPA had one or more functional group(s) large enough to collide with MAO-B (Figure 1A,B) but not preclude binding to LSD1, based on our structural superimposition (Figure 1C,D). In the 2-PCPA with fluorines, we observed two major steric hindrances at Y398 and F343, and another from the opposite direction at Q206, in MAO-B (Figure 1A,B). On the other hand, there were minimal clashes with the hypothetical fluorine in LSD1 (Figure 1C,D), where the only collision was expected with T335, which was small and thus less serious in comparison to those in MAO-B.

We synthesized this 2-PCPA compound with fluorines at sites R_1, R_2, R_3, R_4, and R_6, to form *trans*-2-pentafluorophenylcyclopropylamine hydrochloride, designated 2-PFPA (Figure 2), and performed an inhibitory assay with LSD1, using the peroxidase assay system (Figure 3 and Figure S2 of the Supporting Information). The slow-binding inhibitor equation was used to calculate the inhibition kinetics, because the assay data fit significantly better to it than to the Michaelis−Menten equation (*26*, *30*). 2-PFPA showed a 5.5-fold k_{inact}/K_I increase for LSD1 inhibition as compared to that of 2-PCPA, with a k_{inact}/K_I value of 321 M^{-1} s^{-1} in the peroxidase-coupled reaction (Table 1). On the other hand, the level of MAO-A inhibition decreased 40-fold in k_{inact}/K_I (Table 1), indicating that the extra fluorines were sufficient to repel MAO-A and supporting the validity of the model. However, the level of MAO-B inhibition increased by 1.5-fold in k_{inact}/K_I (Table 1), implying that the MAO-B reactive cavity is quite flexible and willingly accepts these hypothetical hindrances. Although we were able to reverse the specificity of 2-PFPA from MAO-A to LSD1, 2-PFPA inhibits MAO-B with a k_{inact}/K_I value of 409 M^{-1} s^{-1} (Table 1).

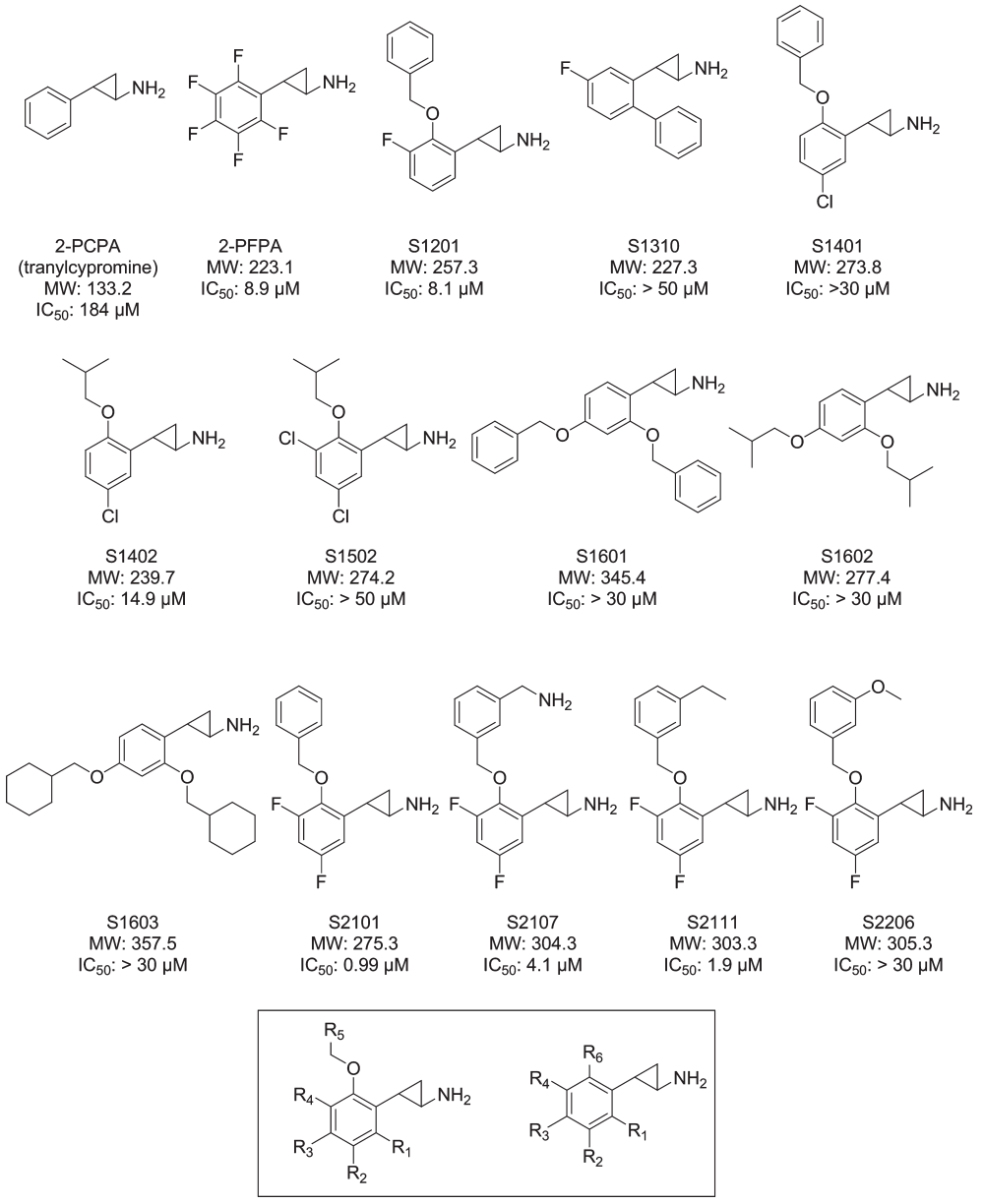

FIGURE 2: Representative 2-PCPA derivatives used in this study. The molecular mass and IC_{50} value of each compound are shown. 2-PCPA derivatives that exhibited IC_{50} values of $> 30\,\mu M$ were excluded from further kinetic analyses to determine the k_{inact}/K_I values. All compounds are *trans* isomers and react in a fashion similar to that of 2-PCPA.

Structural Analysis of 2-PFPA-Inhibited LSD1. To gain molecular insight into the LSD1 inhibition by 2-PFPA, we determined the crystal structure of 2-PFPA-bound LSD1 at 3.2 Å (Figure 4A and Table S1 of the Supporting Information). Although the resolution was not sufficiently high for the compound structures, the 2.25 Å inhibitor-free LSD1 structure used as a molecular replacement model (*27*) was sufficient to yield well-phased maps for the extra protrusion. We were not able to distinguish between the five-membered ring model and the N(5) model at this resolution, so the five-membered ring model was used. We found that the cyclopropyl group of 2-PFPA was fused to FAD in the catalytic center of LSD1, presumably via a mechanism similar to that of 2-PCPA-mediated inactivation of LSD1, with five fluorines protruding from the phenyl ring of 2-PFPA (Figure 4A). An examination of the surrounding LSD1 residues in this complex revealed that the fluorines stabilized the phenyl ring position of 2-PFPA by limiting its torsion angle, thus preventing it from twisting past Y761 of LSD1 (Figure 4B). A comparison of the inhibitory residues with those of the 2-PCPA structure showed that the residues around FAD, such as I356, V333, Y761, T335, L706, and F538, had moved slightly away from the reactive cavity, suggesting that the reactive cavity creates more space to accommodate the extra fluorine atoms (Figure 4C).

Design and Inhibition Analysis of 2-PCPA Derivatives. We next designed 2-PCPA derivatives with bulky, hydrophobic groups, such as phenyl rings, at the *ortho* positions of 2-PCPA, because the *ortho* site is the location where the fluorines distinguished LSD1 from MAO-B (Figure 5). The *ortho*-substituted 2-PCPA derivatives were expected to be better LSD1 inhibitors, since the substitution at the *ortho* positions would exhibit drastic hindrance with MAO-B, but little with LSD1. In the hypothetical structure of the compound S1000, Y398 as well as Y435 of MAO-B exhibited severe hindrance with the inhibitor from both sides, leaving little space for the closed MAO-B reaction cavity to reorient and accept this inhibitor (Figure 5A,B). Although this

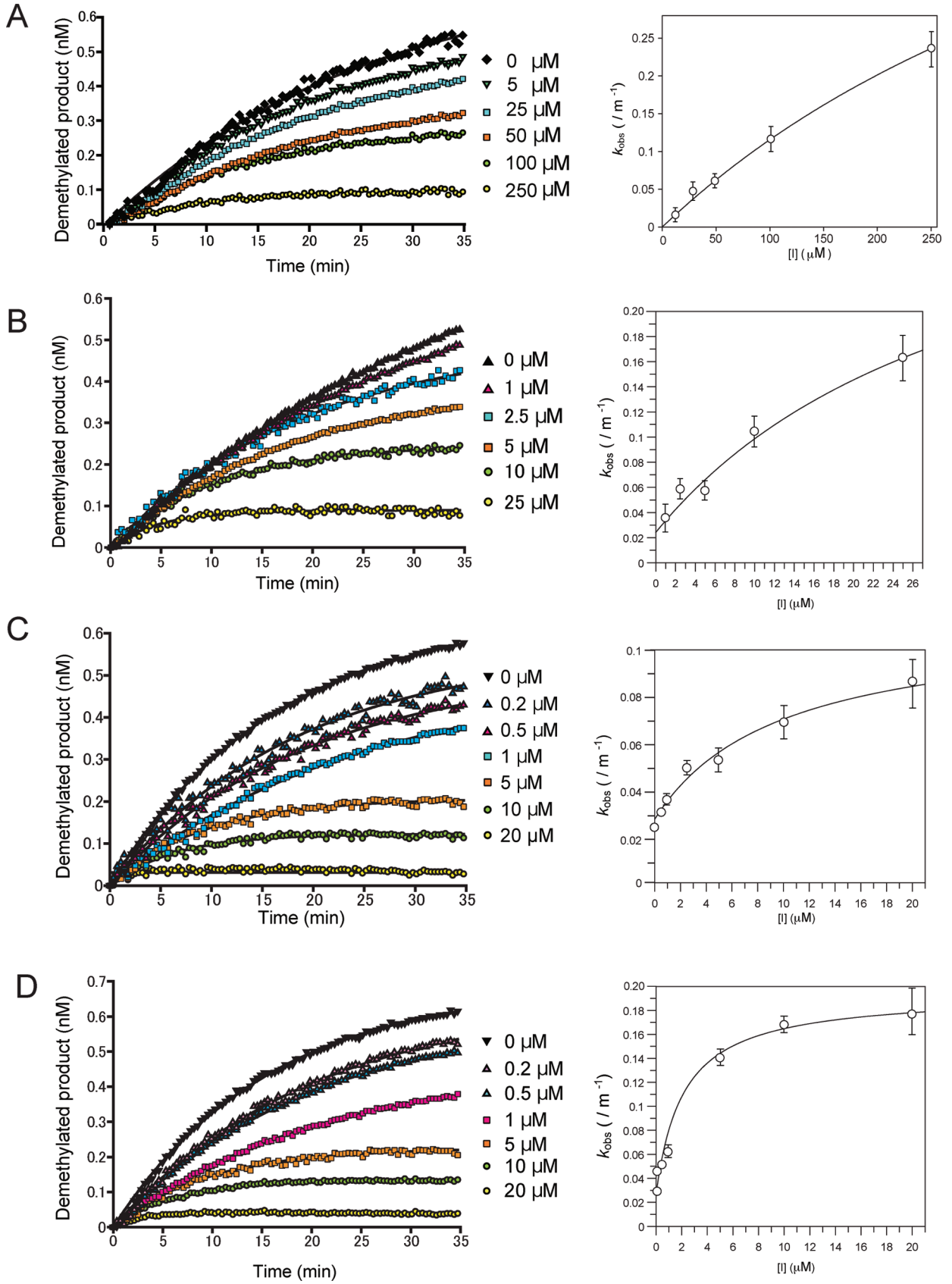

FIGURE 3: Time course inhibition analyses of LSD1. Time course inhibition data (left) and Kitz−Wilson plots (right) are shown for (A) 2-PCPA, (B) 2-PFPA, (C) S1201, and (D) S2101. All assays were performed using the peroxidase assay system, using Modified Trinder's reagent as a color producer, and H3K4me2 peptides (corresponding to residues 1−20). The LSD1 demethylation inhibition became gradually stronger as the compound generation progressed from the initial 2-PCPA to S2101.

hypothetical compound exhibited hindrance with Y761 of LSD1 (Figure 5C,D), we presumed that the LSD1 reactive cavity could accept this amount of steric hindrance, based on the 2-PFPA structure and the demethylation assays, because the hindrance is

Table 1: Kinetic Parameters for Inhibition by the 2-PCPA Derivatives

inhibitor	k_{inact} (s^{-1})	K_I (μM)	k_{inact}/K_I (M^{-1} s^{-1})
	LSD1		
S2101	$0.0028 \pm 1.01 \times 10^{-4}$	0.61 ± 0.13	4560
S2107	$0.0034 \pm 8.65 \times 10^{-4}$	1.6 ± 0.17	2070
S2111	$0.0045 \pm 6.50 \times 10^{-4}$	1.5 ± 0.67	2990
S1402	$0.0017 \pm 6.60 \times 10^{-4}$	3.8 ± 1.4	458
S1201	$0.0011 \pm 1.20 \times 10^{-4}$	2.4 ± 0.63	447
2-PFPA	$0.0054 \pm 1.80 \times 10^{-4}$	17 ± 4.9	321
2-PCPA	$0.0060 \pm 6.20 \times 10^{-4}$	100 ± 22	58
	MAO-B		
S2101	$0.00032 \pm 3.50 \times 10^{-5}$	17 ± 2.5	18
S2107	$0.00013 \pm 1.00 \times 10^{-5}$	27 ± 3.3	5.0
S2111	$0.00024 \pm 2.00 \times 10^{-5}$	5.1 ± 1.1	49
S1402	$0.00055 \pm 7.33 \times 10^{-5}$	44 ± 8.7	13
S1201	$0.00050 \pm 1.45 \times 10^{-4}$	42 ± 24	12
2-PFPA	$0.0034 \pm 1.17 \times 10^{-3}$	8.3 ± 0.083	409
2-PCPA	$0.0071 \pm 2.00 \times 10^{-4}$	26 ± 0.082	271
	MAO-A		
S2101	$0.0065 \pm 2.83 \times 10^{-4}$	110 ± 11	60
S2107	$0.0012 \pm 1.83 \times 10^{-5}$	150 ± 5.4	8.0
S2111	$0.0057 \pm 6.50 \times 10^{-4}$	27 ± 5.9	210
S1402	$0.0038 \pm 9.00 \times 10^{-4}$	37 ± 9.6	102
S1201	$0.0049 \pm 7.50 \times 10^{-4}$	64 ± 17	76
2-PFPA	$0.0071 \pm 9.00 \times 10^{-4}$	270 ± 30	26
2-PCPA	$0.0056 \pm 6.50 \times 10^{-4}$	5 ± 0.70	1050

only from one direction and is within 1−2 Å. Our attempt to synthesize the compound S1000 was unsuccessful, probably because of insolubility during the synthesis (Figure 5E). Therefore, we synthesized eight derivatives of this type, most with *ortho* extensions of the phenyl ring, and some with halogen modifications [i.e., S1201 to S1603 (see Figure 2)]. Throughout this study, all of the synthesized 2-PCPA derivatives were *trans* isomers. These compounds have a combination of fluoro-, chloro-, phenyl-, isobutoxy-, benzyloxy-, and cyclohexylmethoxy groups at either the *ortho*, *meta*, or *para* position of the phenyl ring. Using the peroxidase-coupled reaction method, we screened these compounds and determined their IC_{50} values (Figure 2). This screening identified two compounds, S1201 and S1402, with IC_{50} values of < 20 μM. S1201 and S1402 both inhibited LSD1, with k_{inact}/K_I values of 447 and 458 M^{-1} s^{-1}, respectively (Table 1 and Figure 3). The LSD1 inhibition activity, measured by k_{inact}/K_I, increased 7.7- and 7.9-fold for S1201 and S1402 toward 2-PCPA, respectively, and these values are slightly higher than the activity of 2-PFPA (Table 1 and Table S2 of the Supporting Information). The inhibitory statistics to MAO-A and MAO-B are summarized in Table 1.

A comparison of the derivatives S1201 and S1402 revealed that the R_6 position with a benzyloxy group (S1201) showed greater inhibition than that with an isobutoxy group (S1402) (Figure 2). They displayed similar hindrance of MAO-B, showing that both modifications repel MAO-B residues in the reactive cavity to the same extent but favor the benzyloxy group in LSD1. The reactivity of compound S1201 to MAO-A and MAO-B was decreased 14- and 23-fold relative to 2-PCPA, respectively, with k_{inact}/K_I values of 76 and 12 M^{-1} s^{-1}, respectively (Table 1). The decreased level of MAO inhibition is quite consistent with the initial superimpositions of the 2-PCPA-inhibited structures of LSD1 and MAO-B, although it is surprising that the MAO reaction cavity accepts the inhibitors that were designed with

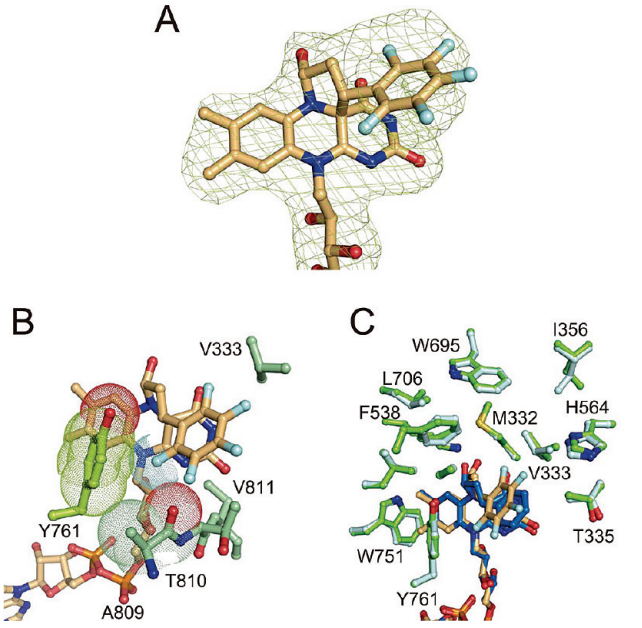

FIGURE 4: Crystal structure of the LSD1−2-PFPA complex. (A) An $F_o - F_c$ omit map contoured at 3σ, omitting the FAD−2-PFPA adduct formed in the LSD1 reactive cavity. The electron density was well-phased, using the 2.25 Å structure of inhibitor-free LSD1 as a molecular replacement model. (B) Structural environment of the LSD1−2-PFPA complex. Surrounding LSD1 residues are colored green. The phenyl ring of 2-PFPA is notably stabilized by Y761, which prevents it from twisting. Other residues, such as V333 and A809, contribute to the stability of the adduct structure. (C) Structural comparisons of 2-PCPA−LSD1 and 2-PFPA−LSD1 complexes. The 2-PCPA adduct is colored blue, and the 2-PFPA adduct is colored orange. The residues surrounding the 2-PCPA−LSD1 complex are colored cyan, and those surrounding the 2-PFPA−LSD1 complex are colored green. The residues surrounding LSD1 shift to a more open conformation in general to accept the extra fluorine, and especially, I356 adopts a different orientation. In addition, the adduct structure adopts a slightly different orientation.

steric obstructions. Significant improvements in LSD1 inhibition were not observed when the R_3 moiety (i.e., *para* position) was substituted, as in compounds S1601, S1602, and S1603, with both phenyl and alkyl modifications, suggesting that *para* modifications of 2-PCPA are redundant (Figure 2).

Structural Analysis of S1201-Inhibited LSD1. To investigate the inhibitory binding mode of the 2-PCPA derivatives, we determined the crystal structure of LSD1 inhibited by the hit compound, S1201, at 3.1 Å (Figure 6A and Table S1 of the Supporting Information). The LSD1−S1201 complex was structurally stable, and the central phenyl ring of compound S1201 could not twist, because of the presence of the benzyloxy group at the R_6 position (Figure 6B). This protruding phenyl moiety at the *ortho* position is hydrophobically stabilized by the surrounding LSD1 residues, such as V333, F538, and L539, and is further sterically stabilized by H564 (Figure 6B). Thus, the strong LSD1 inhibition activity of S1201 is mainly attributable to the additional interactions formed between the protruding phenyl moiety at the *ortho* position of the 2-PCPA derivatives and the inner surface of the LSD1 catalytic center. Surprisingly, the surrounding LSD1 residues in the LSD1−S1201 structure moved only modestly in comparison to those in the 2-PCPA-inhibited LSD1 structure, where the hydrophobic residues gather around the extra phenyl ring of the S1201 adduct (Figure 6C).

Design and Inhibition Analysis of S1201 Derivatives. On the basis of the structure of S1201, we further synthesized four

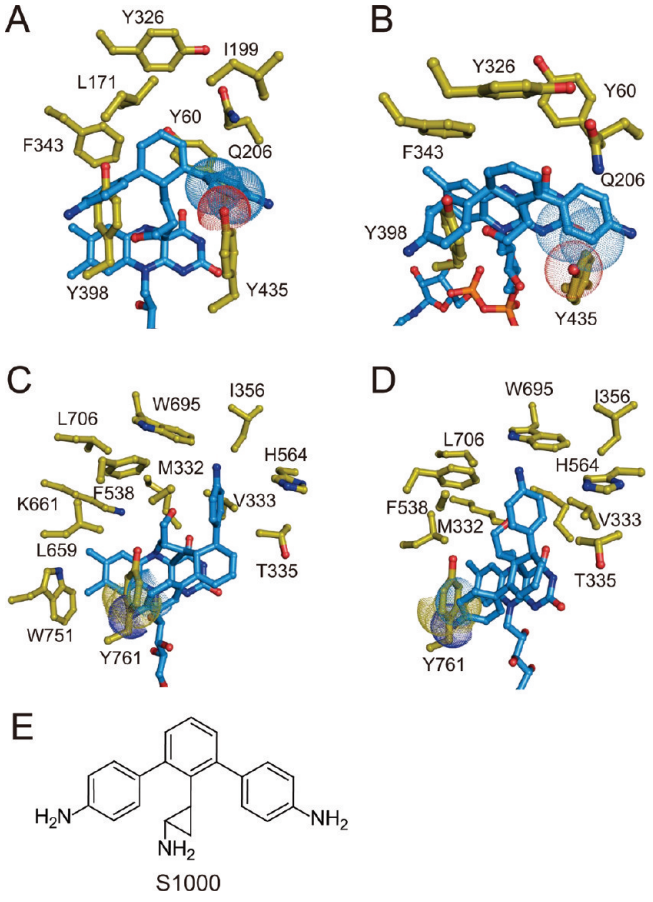

FIGURE 5: Structural comparisons of MAO-B and LSD1 with a 2-PCPA derivative modified at both *ortho* positions. (A) Structural model of MAO-B with a 2-PCPA derivative modified at both *ortho* positions. (B) Structure rotated vertically by 30° from panel A. (C) Structural model of LSD1 with the same 2-PCPA derivative. (D) Structure rotated horizontally by 30° from panel C. (E) Chemical structure of the 2-PCPA derivative, S1000. Dotted spheres represent hypothetical steric clashes. Yellow residues represent surrounding enzyme residues, and blue atoms represent the S1000-FAD adduct. Note that Y398 of MAO-B clashes drastically with this adduct, as does Y435 from the opposite side, suggesting a major obstacle for the 2-PCPA derivatives to react in this compound. The LSD1 adduct clashes with Y761, but we predicted that LSD1 would accept this minute hindrance, on the basis of the previous experiment with 2-PFPA.

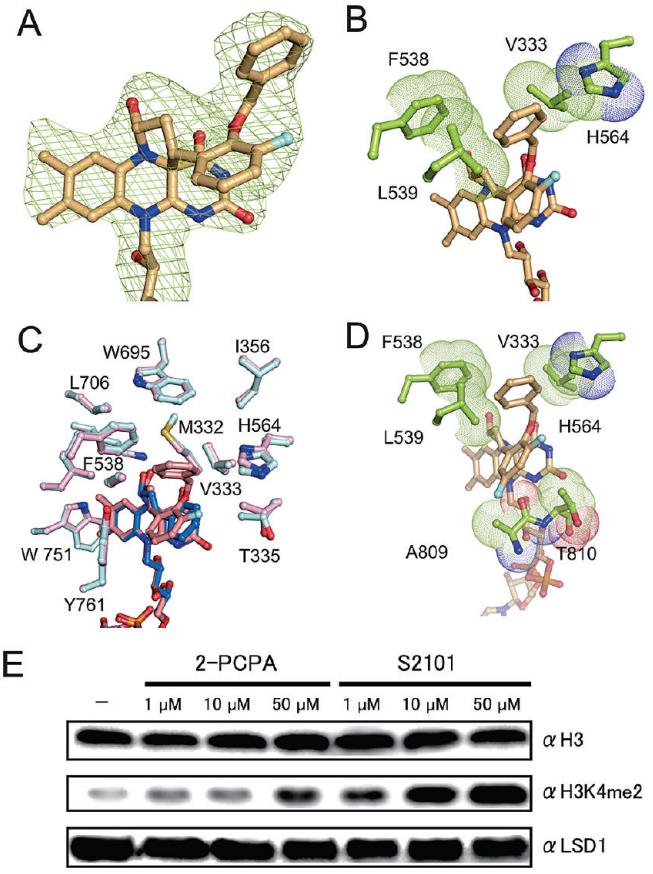

FIGURE 6: Crystal structure of the LSD1−S1201 complex. (A) $F_o - F_c$ omit map of S1201 contoured at 3σ. The FAD-S1201 adduct was omitted for the sake of clarity. The electron density revealed the extra phenyl ring fused to the R_5 *ortho* position of 2-PCPA. (B) Structural environment of the LSD1−S1201 complex. The residues surrounding LSD1 are colored green, and the fluorine is colored cyan. The modified phenyl ring protruding from S1201 is stabilized hydrophobically by the surrounding LSD1 residues V333, F538, L539, and H564. (C) Structural comparison of 2-PCPA−LSD1 and S1201−LSD1 complexes. The 2-PCPA adduct is colored blue, and the S1201 adduct is colored pink. The residues surrounding the 2-PCPA−LSD1 complex are colored cyan, and those surrounding the S1201−LSD1 complex are colored light pink. Residues F538, M332, and I356 move closer to the phenyl ring of the adduct. (D) Proposed structural environment model of the LSD1−S2101 complex. An extra fluorine atom was added to the S1201 structure, to create the S2101−LSD1 complex model. LSD1 residues A809 and T810 additionally contribute to the stability of the adduct. (E) Detection of H3K4me2 levels in S2101-treated HEK293T cells. Cells were incubated with the indicated concentrations of 2-PCPA or S2101 for 24 h, and nuclear extract fractions from each treatment were analyzed by Western blotting with the indicated antibodies.

S1201 derivatives (i.e., S2101, S2107, S2111, and S2206) and screened their LSD1 inhibition activities. We found three compounds, S2101, S2107, and S2111, with IC_{50} values below that of S1201 (Figure 2). Kinetic inhibition assays revealed that S2101, S2107, and S2111 inhibited LSD1 with k_{inact}/K_I values of 4560, 2070, and 2990 M^{-1} s^{-1}, respectively (Table 1). Other kinetic inhibition parameters, including the results of MAO-A and MAO-B inhibitory assays, are summarized in Table 1.

As expected, LSD1 inhibition by the 2-PCPA derivatives was further enhanced when the R_2 or R_4 position (i.e., *meta* positions) was substituted with fluorine (Table 1; see also Figure 2). The activities of the two S1201-based inhibitors, S2101 and S2111, with LSD1 were increased by 79- and 52-fold compared to that of 2-PCPA and 10.2- and 6.7-fold compared to that of S1201, respectively (Table 1). The level of LSD1 inhibition was increased by 1 order of magnitude from that of S1201. The compound S2101 is among the most potent small LSD1 inhibitors reported so far, with K_I values of < 1 μM. This strong LSD1 inhibition is presumably caused by the increased number of hydrophobic interactions of the compound with LSD1 by the novel protruding atoms, and by the fluorines at the *meta* position. The fluorine at the R_2 position decreased the level of MAO-B inhibition relative to 2-PCPA by 15- and 6-fold and decreased the level of MAO-A inhibition by 18- and 5-fold for the inhibitors S2101 and S2111, respectively. These results imply that although the inhibitors react with MAO-A and MAO-B, they are less stable in the reactive cavity. Compounds with other halogens at R_2 and R_4 were also tested in the previous step (i.e., S1401 and S1502); however, both compounds lacked significant improvements in LSD1 inhibition (Figure 2). If we assume that the S2101 structure is similar to that of S1201 with an extra fluorine at the R_2 *meta* position, then S2101 can also be stabilized by A809 and T810 of LSD1, which support the extra fluorine and form hydrophobic

interactions (Figure 6D). Finally, to verify the effects of the inhibitors in this study in cells, we treated HEK293T cells with our most potent inhibitor, S2101, and observed the methylation status of H3K4 by Western blotting. Consistent with our biochemical and structural analyses, the treatment of HEK293T cells with S2101 resulted in a dose-dependent increase in the level of H3K4me2 (Figure 6E), which must have accumulated by the inactivation of LSD1. During the course of the compound treatment, the amounts of histone H3 and LSD1 in the nuclear extracts remained essentially unaffected (Figure 6E). Because the treatment with 1 μM S2101 generated a level of H3K4me2 similar to that elicited by 50 μM 2-PCPA, S2101 is assumed to have approximately 50-fold stronger LSD1 inhibition activity than 2-PCPA in human cells.

DISCUSSION

Several epigenetic drugs, such as HDAC-inhibiting trichostatin A (TSA) and suberolyanilide hydroxamic acid (SAHA), are reportedly effective in various malignancies, such as breast cancer, multiple myeloma, and cutaneous T-cell lymphoma (CTCL) (*37*). The structures of TSA and SAHA were also determined and revealed that both drugs fit remarkably well in the reactive cavity (*38*). On the other hand, DNA methyltransferase inhibitors, such as 5-azacytidine and 5-aza-2′-deoxycytidine, are known to be effective in myelodysplastic syndrome (MDS) (*39*). These inhibitors have proven that epigenetic inhibitors are useful drug candidates. Therefore, histone demethylase inhibitors would also be clinically useful for cancers and various syndromes. Currently, LSD1 is known to function in prostate cancer, and its polyamine analogues have an effect on colon cancer, as well as latent virus infections (*20*−*22*). In this study, we have achieved two objectives through structural and biochemical analyses: (1) improvement of the selectivity toward LSD1 and (2) significant enhancement of the inhibition efficiency. Structure-based drug design has an advantage in the direct knowledge of the drug target (*40*). We have reduced the number of candidate compounds to a little more than a dozen, reached submicromolar level inhibition, and increased the specificity further by weakening the drug's inhibition of MAO-A and MAO-B. The crystal structures we obtained in this study enabled us to gain insight into each step of the inhibitor construction campaign of LSD1 and to accomplish the next step of efficiently improving the candidate compounds by predicting potential bonds, stabilizing factors, and obstructions.

Our inhibitor design involved structurally obstructing the residues in the reactive cavities of the enzymes, while simultaneously stabilizing the residues inside the reactive cavity of the target enzyme. The compounds were designed three times, via comparison of the structure of LSD1 inhibited by one of the potent inhibitors, and that of MAO-B. As seen with our first compound, 2-PFPA, the steric clashes in MAO-B at Y398 and Q206 obstructed 2-PFPA from both sides (Figure 1). On the other hand, when 2-PFPA was superimposed in LSD1, there were minimal clashes, except at T335. The second generation of compounds was designed from 2-PFPA to sterically obstruct MAO-B completely, while improving LSD1 inhibition. We successfully obtained two derivatives, S1201 and S1402, that have a benzyloxy or an isobutoxy group at the R_6 position (Figure 2). Finally, we synthesized S1201-based derivatives by adding fluorines and obtained two hit compounds, S2101 and S2111. S2101 showed the best inhibition, with a k_{inact}/K_I value of 4560 M^{-1} s^{-1}, which is 79 times stronger than that of 2-PCPA, resulting in the most LSD1-potent and -specific compound (Table 1). Interestingly, the Kitz−Wilson plots of the 2-PCPA derivatives developed in this study showed a non-zero *y*-intercept, suggesting the possibility that the inhibitors may slowly dissociate from LSD1 (Figure 3B−D). These 2-PCPA derivatives may form a transient intermediate with LSD1 before they react with LSD1-FAD, although we cannot exclude the possibility that the reacted FAD adducts slowly dissociate from LSD1. This nonzero *y*-intercept was not detected when the compounds were investigated with MAOs. On the other hand, compounds such as S1401, S1502, S1601, S1602, and S1603 were found to be poor LSD1 inhibitors, with IC_{50} values of > 30 μM (Figure 2). Thus, the substitution of chlorine, which is larger than fluorine, may be too large for the LSD1 inhibition, and the substitution of the *para* position is assumed to be insignificant for the inhibition (Figure S3A of the Supporting Information).

We structurally validated the improved inhibition of the compounds each time, by determining their crystal structures in complex with LSD1, or creating a model based on a related structure. When the 2-PFPA−LSD1 complex structure was compared to that of 2-PCPA-inhibited LSD1, the LSD1 residues around the reactive cavity, such as W751, W695, I356, H564, V333, T335, Y761, and F538, shifted to increase the area of the reactive cavity to accept the larger adduct, 2-PFPA (Figure 4C). The LSD1−S1201 complex structure showed the increased stability of the LSD1-FAD−S1201 adduct, in which the phenyl ring at the R_2 site is stabilized by hydrophobic interactions with the surrounding LSD1 residues F538, L539, V333, and H564 (Figure 6A,B). A comparison of these residues to those surrounding 2-PCPA revealed that the F538, I356, and M332 residues moved closer to the phenyl ring of the adduct, providing evidence of the improved stabilization of the phenyl ring at the R_5 site (Figure 6C). We built the structural model of the S2101-inhibited LSD1 complex by adding the extra fluorine in S2101 to S1201 and found that the LSD1 residues A809 and T810 further stabilized the inhibitory structure (Figure 6D). A superposition of all three LSD1 structures inhibited by 2-PCPA, 2-PFPA, and S1201 revealed that the surrounding LSD1 residues shifted the most in 2-PFPA, and the hydrophobic residues F538, I356, and V333 gathered around the extra phenyl ring in S1201 (Figure S3B of the Supporting Information).

Considering the >250-fold difference in the inhibition of LSD1 and MAO-B by S2101, we believe that this structurally improved inhibitor is one of the most potent small molecule inhibitors of LSD1 discovered to date. Indeed, we demonstrated that S2101 exhibits approximately 50-fold stronger LSD1 inhibition than 2-PCPA in human cells (Figure 6E). However, we can envision further improvements. This inhibitor mostly forms a covalent bond with the LSD1-FAD adduct, which inevitably inhibits the enzyme permanently and could be improved via substitution of the cyclopropane ring with a noncovalent inhibitor moiety that can interact with LSD1-FAD. Another essential factor for inhibitors is their cellular permeability, to allow them to act upon the target. According to Lipinski's rules of five, a molecular mass of < 500 Da is a preferable feature for a drug, since a larger molecule would have a greater likelihood of unfavorable interactions with cellular proteins (*41*). The 2-PCPA derivatives in this study have an advantage in that they are well below the limit for permeability, since the masses of all of the inhibitors are below 310 Da, allowing easy access to the nucleus, where LSD1 is expressed. The polyamine analogues of the H3 tail

are noncovalent inhibitors and thus have an advantage over the covalently reacting 2-PCPA derivatives. However, the 2-PCPA derivatives presented in this study have molecular masses much smaller than those of the known LSD1 inhibitors, suggesting their favorable disposition.

Recently, three reports regarding LSD1 inhibitors were published (*42*−*44*). One described 2-PCPA-based compounds with a K_I value of 3.1 μM and a k_{inact}/K_I value of 2000 M^{-1} s^{-1} toward LSD1 at maximum (*42*). The second report described histone H3 peptide derivatives (residues 1−21 of H3) with FAD-inactivating functional groups, with a K_I value of 0.00435 μM and a k_{inact}/K_I value of 56.8 μM^{-1} min^{-1} toward LSD1 at maximum (*43*). The third report described *para* 2-PCPA derivatives that were useful with both LSD1 and LSD2 (*44*). According to Ueda et al., the *para* modifications of the phenyl ring of 2-PCPA improved the LSD1 inhibition when the modification was extended, to mimic the histone peptide (*42*). The effect of an *ortho* substitution was not examined in these three reports (*42*−*44*). Still, our compounds with *ortho* modifications showed submicromolar inhibition despite their size, indicating the significance of the *ortho* modifications for the rational design of small and robust LSD1 inhibitors.

CONCLUSIONS

In this study, we have rationally developed novel LSD1 inhibitors based on the superimpositions of the 2-PCPA-inhibited structures of LSD1 and MAO-B. Through three rounds of compound screening and determination of the 2-PFPA- and S1201-inhibited LSD1 structures, we obtained the small, potent LSD1 inhibitor, S2101, which has a K_I value of <1 μM. Our crystal structure analyses indicated that the addition of a phenyl ring at the *ortho* moiety of the 2-PCPA phenyl ring was quite effective for LSD1 inhibition, through its stabilization by the surrounding LSD1 residues. As a result of the significant increase in the level of LSD1 inhibition, reaching submicromolar levels, and the decrease in the level of MAO inhibition, presumably through the designed steric hindrance, the modified 2-PCPA derivatives increased the inhibitor's specificity for LSD1. The derivatives would have the advantage of cellular permeability in comparison to other LSD1 inhibitors, because of their low molecular masses. The LSD1 inhibitors described in this study will provide functional and structural bases for the development of carcinoma-treating and/or anti-infective drugs as well as the advancement of epigenetic research.

ACKNOWLEDGMENT

We thank Drs. K. Machida, Y. Hirose, and H. Suzuki (ChemGenesis, Inc.) for chemical synthesis; Y. Kondo and N. Yamaguchi (Toray Research Center, Inc.) for peptide synthesis; S. Sekine, T. Ito, T. Sengoku, and Y. Fujii for structural assistance; the BL26B2 and BL41XU beamline staff at SPring-8 for data collection (Proposals 20080052 and 20090007); M. Wakiyama, M. Ikeda, Y. Yoneyama, and S. Takahashi (The University of Tokyo) for cell culture; and T. Nakayama, A. Ishii, S. Saito, H. Kato, and K. Shinozaki for clerical assistance.

SUPPORTING INFORMATION AVAILABLE

Detailed experimental procedures of compound synthesis, a table of MAO-A and MAO-B assays, and X-ray data collection and refinement statistics. This material is available free of charge via the Internet at http://pubs.acs.org.

REFERENCES

1. Strahl, B. D., and Allis, C. D. (2000) The language of covalent histone modifications. *Nature 403*, 41–45.
2. Taverna, S. D., Li, H., Ruthenburg, A. J., Allis, C. D., and Patel, D. J. (2007) How chromatin-binding modules interpret histone modifications: Lessons from professional pocket pickers. *Nat. Struct. Mol. Biol. 14*, 1025–1040.
3. Tachibana, M., Sugimoto, K., Nozaki, M., Ueda, J., Ohta, T., Ohki, M., Fukuda, M., Takeda, N., Niida, H., Kato, H., and Shinkai, Y. (2002) G9a histone methyltransferase plays a dominant role in euchromatic histone H3 lysine 9 methylation and is essential for early embryogenesis. *Genes Dev. 16*, 1779–1791.
4. Shinkai, Y. (2007) Regulation and function of H3K9 methylation. *Subcell. Biochem. 41*, 337–350.
5. Swigut, T., and Wysocka, J. (2007) H3K27 demethylases, at long last. *Cell 131*, 29–32.
6. Guenther, M. G., Jenner, R. G., Chevalier, B., Nakamura, T., Croce, C. M., Canaani, E., and Young, R. A. (2005) Global and Hox-specific roles for the MLL1 methyltransferase. *Proc. Natl. Acad. Sci. U.S.A. 102*, 8603–8608.
7. Iwase, S., Lan, F., Bayliss, P., de la Torre-Ubieta, L., Huarte, M., Qi, H. H., Whetstine, J. R., Bonni, A., Roberts, T. M., and Shi, Y. (2007) The X-linked mental retardation gene SMCX/JARID1C defines a family of histone H3 lysine 4 demethylases. *Cell 128*, 1077–1088.
8. Shi, Y., Lan, F., Matson, C., Mulligan, P., Whetstine, J. R., Cole, P. A., and Casero, R. A. (2004) Histone demethylation mediated by the nuclear amine oxidase homolog LSD1. *Cell 119*, 941–953.
9. Culhane, J. C., and Cole, P. A. (2007) LSD1 and the chemistry of histone demethylation. *Curr. Opin. Chem. Biol. 11*, 561–568.
10. Forneris, F., Binda, C., Battaglioli, E., and Mattevi, A. (2008) LSD1: Oxidative chemistry for multifaceted functions in chromatin regulation. *Trends Biochem. Sci. 33*, 181–189.
11. Forneris, F., Binda, C., Vanoni, M. A., Mattevi, A., and Battaglioli, E. (2005) Human histone demethylase LSD1 reads the histone code. *FEBS Lett. 579*, 2203–2207.
12. Yang, M., Gocke, C. B., Luo, X., Borek, D., Tomchick, D. R., Machius, M., Otwinowski, Z., and Yu, H. (2006) Structural basis for CoREST-dependent demethylation of nucleosomes by the human LSD1 histone demethylase. *Mol. Cell 23*, 377–387.
13. Lee, M. G., Wynder, C., Cooch, N., and Shiekhattar, R. (2005) An essential role for CoREST in nucleosomal histone 3 lysine 4 demethylation. *Nature 437*, 432–435.
14. Gu, H., and Roizman, B. (2009) Engagement of the lysine-specific demethylase/HDAC1/CoREST/REST complex by herpes simplex virus 1. *J. Virol. 83*, 4376–4385.
15. Lan, F., Collins, R. E., De Cegli, R., Alpatov, R., Horton, J. R., Shi, X., Gozani, O., Cheng, X., and Shi, Y. (2007) Recognition of unmethylated histone H3 lysine 4 links BHC80 to LSD1-mediated gene repression. *Nature 448*, 718–722.
16. Metzger, E., Wissmann, M., Yin, N., Muller, J. M., Schneider, R., Peters, A. H., Gunther, T., Buettner, R., and Schule, R. (2005) LSD1 demethylates repressive histone marks to promote androgen-receptor-dependent transcription. *Nature 437*, 436–439.
17. Huang, J., Sengupta, R., Espejo, A. B., Lee, M. G., Dorsey, J. A., Richter, M., Opravil, S., Shiekhattar, R., Bedford, M. T., Jenuwein, T., and Berger, S. L. (2007) p53 is regulated by the lysine demethylase LSD1. *Nature 449*, 105–108.
18. Wang, J., Hevi, S., Kurash, J. K., Lei, H., Gay, F., Bajko, J., Su, H., Sun, W., Chang, H., Xu, G., Gaudet, F., Li, E., and Chen, T. (2009) The lysine demethylase LSD1 (KDM1) is required for maintenance of global DNA methylation. *Nat. Genet. 41*, 125–129.
19. Wang, Y., Zhang, H., Chen, Y., Sun, Y., Yang, F., Yu, W., Liang, J., Sun, L., Yang, X., Shi, L., Li, R., Li, Y., Zhang, Y., Li, Q., Yi, X., and Shang, Y. (2009) LSD1 is a subunit of the NuRD complex and targets the metastasis programs in breast cancer. *Cell 138*, 660–672.
20. Huang, Y., Greene, E., Murray Stewart, T., Goodwin, A. C., Baylin, S. B., Woster, P. M., and Castero, R. A., Jr. (2007) Inhibition of lysine-specific demethylase 1 by polyamine analogues results in re-expression of aberrantly silenced genes. *Proc. Natl. Acad. Sci. U.S.A. 104*, 8023–8028.
21. Huang, Y., Stewart, T. M., Wu, Y., Baylin, S. B., Marton, L. J., Perkins, B., Jones, R. J., Woster, P. M., and Casero, R. A., Jr. (2009) Novel oligoamine analogues inhibit lysine-specific demethylase 1 and induce reexpression of epigenetically silenced genes. *Clin. Cancer Res. 15*, 7217–7228.
22. Liang, Y., Vogel, J. L., Narayanan, A., Peng, H., and Kristie, T. M. (2009) Inhibition of the histone demethylase LSD1 blocks α-herpesvirus lytic replication and reactivation from latency. *Nat. Med. 15*, 1312–1317.

23. Lee, M. G., Wynder, C., Schmidt, D. M., McCafferty, D. G., and Shiekhattar, R. (2006) Functional interplay between histone demethylase and deacetylase enzymes. *Chem. Biol. 13*, 563–567.
24. Schmidt, D. M., and McCafferty, D. G. (2007) *trans*-2-Phenylcyclopropylamine is a mechanism-based inactivator of the histone demethylase LSD1. *Biochemistry 46*, 4408–4416.
25. Gooden, D. M., Schmidt, D. M., Pollock, J. A., Kabadi, A. M., and McCafferty, D. G. (2008) Facile synthesis of substituted trans-2-arylcyclopropylamine inhibitors of the human histone demethylase LSD1 and monoamine oxidases A and B. *Bioorg. Med. Chem. Lett. 18*, 3047–3051.
26. Yang, M., Culhane, J. C., Szewczuk, L. M., Jalili, P., Ball, H. L., Machius, M., Cole, P. A., and Yu, H. (2007) Structural basis for the inhibition of the LSD1 histone demethylase by the antidepressant trans-2-phenylcyclopyopylamine. *Biochemistry 46*, 8058–8065.
27. Mimasu, S., Sengoku, T., Fukuzawa, S., Umehara, T., and Yokoyama, S. (2008) Crystal structure of histone demethylase LSD1 and tranylcypromine at 2.25 Å. *Biochem. Biophys. Res. Commun. 366*, 15–22.
28. Schulte, J. H., Lim, S., Schramm, A., Friedrichs, N., Koster, J., Versteeg, R., Ora, I., Pajtler, K., Klein-Hitpass, L., Kuhfittig-Kulle, S., Metzger, E., Schule, R., Eggert, A., Buettner, R., and Kirfel, J. (2009) Lysine-specific demethylase 1 is strongly expressed in poorly differentiated neuroblastoma: Implications for therapy. *Cancer Res. 69*, 2065–2071.
29. Binda, C., Li, M., Hubalek, F., Restelli, N., Edmondson, D. E., and Mattevi, A. (2003) Insights into the mode of inhibition of human mitochondrial monoamine oxidase B from high-resolution crystal structures. *Proc. Natl. Acad. Sci. U.S.A. 100*, 9750–9755.
30. Maurer, T. S., Tabrizi-Fard, M. A., and Fung, H. L. (2000) Impact of mechanism-based enzyme inactivation on inhibitor potency: Implications for rational drug discovery. *J. Pharm. Sci. 89*, 1404–1414.
31. Kitz, R., and Wilson, I. B. (1962) Esters of methanesulfonic acid as irreversible inhibitors of acetylcholinesterase. *J. Biol. Chem. 237*, 3245–3249.
32. Emsley, P., and Cowtan, K. (2004) Coot: Model-building tools for molecular graphics. *Acta Crystallogr. D60*, 2126–2132.
33. Brunger, A. T., Adams, P. D., Clore, G. M., DeLano, W. L., Gros, P., Grosse-Kunstleve, R. W., Jiang, J. S., Kuszewski, J., Nilges, M., Pannu, N. S., Read, R. J., Rice, L. M., Simonson, T., and Warren, G. L. (1998) Crystallography & NMR system: A new software suite for macromolecular structure determination. *Acta Crystallogr. D54*, 905–921.
34. Brunger, A. T. (2007) Version 1.2 of the Crystallography and NMR system. *Nat. Protoc. 2*, 2728–2733.
35. Lovell, S. C., Davis, I. W., Arendall, W. B., III, de Bakker, P. I., Word, J. M., Prisant, M. G., Richardson, J. S., and Richardson, D. C. (2003) Structure validation by Cα geometry: ϕ, ψ and Cβ deviation. *Proteins 50*, 437–450.
36. Muller, K., Faeh, C., and Diederich, F. (2007) Fluorine in pharmaceuticals: Looking beyond intuition. *Science 317*, 1881–1886.
37. Xu, W. S., Parmigiani, R. B., and Marks, P. A. (2007) Histone deacetylase inhibitors: Molecular mechanisms of action. *Oncogene 26*, 5541–5552.
38. Finnin, M. S., Donigian, J. R., Cohen, A., Richon, V. M., Rifkind, R. A., Marks, P. A., Breslow, R., and Pavletich, N. P. (1999) Structures of a histone deacetylase homologue bound to the TSA and SAHA inhibitors. *Nature 401*, 188–193.
39. Patra, S. K., and Bettuzzi, S. (2009) Epigenetic DNA-(cytosine-5-carbon) modifications: 5-Aza-2′-deoxycytidine and DNA-demethylation. *Biochemistry* (*Moscow, Russ. Fed.*) *74*, 613–619.
40. Kuntz, I. D. (1992) Structure-based strategies for drug design and discovery. *Science 257*, 1078–1082.
41. Lipinski, C. A., Lombardo, F., Dominy, B. W., and Feeney, P. J. (2001) Experimental and computational approaches to estimate solubility and permeability in drug discovery and development settings. *Adv. Drug Delivery Rev. 46*, 3–26.
42. Ueda, R., Suzuki, T., Mino, K., Tsumoto, H., Nakagawa, H., Hasegawa, M., Sasaki, R., Mizukami, T., and Miyata, N. (2009) Identification of cell-active lysine specific demethylase 1-selective inhibitors. *J. Am. Chem. Soc. 131*, 17536–17537.
43. Culhane, J. C., Wang, D., Yen, P. M., and Cole, P. A. (2010) Comparative analysis of small molecules and histone substrate analogues as LSD1 lysine demethylase inhibitors. *J. Am. Chem. Soc. 132*, 3164–3176.
44. Binda, C., Valente, S., Romanenghi, M., Pilotto, S., Cirilli, R., Karytinos, A., Ciossani, G., Botrugno, O. A., Forneris, F., Tardugno, M., Edmondson, D. E., Minucci, S., Mattevi, A., and Mai, A. (2010) Biochemical, structural, and biological evaluation of tranylcypromine derivatives as inhibitors of histone demethylases LSD1 and LSD2. *J. Am. Chem. Soc. 132*, 6827–6833.